In-situ and Real-time Monitoring of Mechanochemical Preparation of $Li_2Mg(NH_2BH_3)_4$ and $Na_2Mg(NH_2BH_3)_4$ and their Thermal Dehydrogenation†

Nikola Biliškov,*[a] Andreas Borgschulte,[b] Krunoslav Užarević,[a] Ivan Halasz,[a] Stipe Lukin,[a] Sanja Milošević,[c] Igor Milanović,[a,c] Jasmina Grbović Novaković[c]

For the first time, in-situ monitoring of uninterrupted mechanochemical synthesis of two bimetallic amidoboranes, $M_2Mg(NH_2BH_3)_4$ (M = Li, Na), by means of Raman spectroscopy has been applied. This approach allowed real-time observation of key intermediate phases and a straightforward follow-up of the reaction course. Detailed analysis of time-dependent spectra revealed a two-step mechanism through $MNH_2BH_3 \cdot NH_3BH_3$ adducts as key intermediate phases which further reacted with MgH_2, giving $M_2Mg(NH_2BH_3)_4$ as final products. The intermediates partially take a competitive pathway toward the oligomeric $M(BH_3NH_2BH_2NH_2BH_3)$ phases. The crystal structure of the novel bimetallic amidoborane $Li_2Mg(NH_2BH_3)_4$ was solved from high-resolution powder diffraction data and showed an analogous metal coordination as in $Na_2Mg(NH_2BH_3)_4$, but a significantly different crystal packing. $Li_2Mg(NH_2BH_3)_4$ thermally dehydrogenates releasing highly pure H_2 in the amount of 7 wt% and at a lower temperature then its sodium analogue making it significantly more viable for practical applications.

1 Introduction

In an attempt to find suitable materials for on-board solid state hydrogen storage, significant efforts are put towards ammonia borane (NH_3BH_3, AB), owing to its high gravimetric and volumetric hydrogen content (19.6 wt% and 145 g dm^{-3}, respectively), as well as good stability under ambient conditions.[1] However, practical applications of AB for hydrogen storage are hindered by unfavourable reaction kinetics along with the formation of gaseous ammonia and borazine as side-products of thermal dehydrogenation.[2,3] To improve thermal behaviour of solid AB, three main strategic approaches are employed: restriction of particles size to nanodimensions,[3–6] addition of catalytically active species[7–9] and chemical modification.[10–14] Beneficial influence of any of these actions usually overcome their obvious shortcoming, which is the reduction of hydrogen content relative to pristine AB.

[0a] *Ruđer Bošković Institute, Bijenička c. 54, 10000 Zagreb, Croatia.*
Tel: +385 1 4561084; E-mail: nbilis@irb.hr
[0b] *Swiss Fedaral Institute for Materials Science and Technology (EMPA), Überlandstrasse 129, Dübendorf, Switzerland.*
[0c] *University of Belgrade, Vinča Institute of Nuclear Sciences, Laboratory for Material Sciences, PO Box 522, 11001 Belgrade, Serbia.*
[0†] Electronic Supplementary Information (ESI) available. See DOI: 10.1039/b000000x/

Amidoboranes are a class of compounds derived from substitution of protic hydrogen on the N atom of AB with a metal ion, most often a light alkaline or alkaline-earth metal.[12] It has been demonstrated by both experimental and theoretical studies that dehydrogenation performance of amidoboranes strongly depends on the ionicity and the size of the involved metal cation. Various metal species, having different atomic radii, charge, electronegativity and coordination number, form bonding interactions with the $(NH_2BH_3)^-$ group, enabling tailoring of relevant properties, especially when more than one metal is involved.[15–19]

Several bimetallic amidoboranes of different stoichiometries were prepared by mechanical ball milling.[17–22] Although synthesis by ball milling is attractive due to its efficiency, often evidenced by quantitative and fast reactions occurring in a single step,[23] conducting mechanochemical reactions in closed and oscillating reaction vessels usually prohibited reaction optimisation due to the inability to monitor its course without interrupting the milling process.[24] Consequently, these reactions were usually treated as black-box techniques and were conducted under tentatively chosen conditions. Resorting to ex-situ reaction monitoring, where milling is periodically interrupted for sampling of the reaction mixture is cumbersome, especially in the case of air- and moisture-sensitive hydride materials.

Therefore, the use of in-situ and real-time monitoring would be of great help to overcome the aforementioned problems. Recently, powder X-ray diffraction (PXRD)[25–27] and Raman spectroscopy[28–30] were introduced to study mechanochemical reactions in-situ and in real time. Both methods have shown highly dynamic reaction environments, fast transformations and formation of new phases.[31] The two techniques are complementary and can be employed simultaneously[32], in order to understand the reactions pathways in details. While PXRD is suitable for monitoring of the evolution of bulk crystalline phases, Raman spectroscopy is more appropriate for monitoring of amorphous phases that are developed inside the mechanochemical reaction vessel. Moreover, in-situ Raman spectroscopy is an affordable laboratory technique, unlike in-situ PXRD, which requires access to a synchrotron radiation source.[27]

In our previous work, we thoroughly studied thermal dehydrogenation of AB by means of IR spectroscopy.[11] Here, we apply Raman spectroscopy to monitor mechanochemical synthesis of bimetallic amidoboranes of the general composition $M_2Mg(AB)_4$ (M = Na, Li, (AB) = NH_2BH_3) in-situ and in real time. As a reference system, we took previously reported $Na_2Mg(AB)_4$ (DSMAB),[13,17] to compare its properties and preparation with the novel $Li_2Mg(AB)_4$ (DLMAB).

To the best of our knowledge, this is the first in-situ monitoring of mechanochemical synthesis of materials for solid-state hydrogen storage. Thus far, mechanisms of mechanochemical preparations of materials for solid-state hydrogen storage were mainly deduced from stepwise ex-situ analysis which provides only limited information due to an inherent time delay between sampling and analysis but also due to the fact that sampling may irreproducibly disturb the mechanochemical process (different ball to powder ration, exposure of the system to air etc.).[30,33]

On the other hand, by using in-situ methods, evolution of the explored system can be monitored, including the formation and reactivity of any intermediate phases. Thus, the detailed preparation mechanism of two very perspective systems for solid-state

hydrogen storage will be revealed in this work.

2 Experimental

Materials and synthesis

Ammonia borane, NH_3BH_3 (Sigma-Aldrich, technical grade, 90 %) was used after recrystallisation from diethyl ether, followed by a wash with ethanol.[34] Lithium hydride, LiH (Alfa Aesar, > 97 %), sodium hydride, NaH (Sigma-Aldrich, 95 %) and magnesium hydride, MgH_2 (Sigma-Aldrich, hydrogen storage grade) are used as purchased. Handling of materials were done in an Ar filled MBraun LabMaster 1500 glove box, which ensures ≤ 0.1 ppm O_2 and H_2O, respectively.

Two types of mechanochemical reactors are used for the purposes of this study: 1. Spex 8000M SamplePrep mill/shaker equipped with hardened steel reaction jar, designed in-house and manufactured by Mitar Ltd; 2. an *iST*500 InSolido Technologies mill with PMMA jars, designed and manufactured in-house. Stainless steel balls are used in both experiments. Equal products were obtained regardless of the used setup for milling.

Spex 8000M is used for general preparations of the samples for further characterisations. Stainless steel balls of the mass $m = 2 \times 4\,\mathrm{g} + 2 \times 1.7\,\mathrm{g}$ were used in these experiments. Milling frequency is 875 cycles per minute in figure eight-shape motion, and the applied milling time was 30 min. In all preparations, the mass of reaction mixture was $\sim 250\,\mathrm{mg}$.

InSolido Technologies mill was used for all in-situ monitoring experiments. The reactions are conducted in PMMA milling jars of 14 mL internal volume, transparent for laser beam,[27] and two stainless steel balls of the mass $m = 4\,\mathrm{g} + 1.3\,\mathrm{g}$ are used. This mill applies linear back-and-forth movement geometry, with tunable frequency. We conducted the reactions at 30 Hz. Raman spectra were acquired by an OceanOptics Maya2000Pro spectrometer, equipped with fiber optics probe and a 785 nm laser for excitation from PD-LD. The setup has been previously published and thoroughly disclosed.[27,28] The experimental conditions, i.e. lowered intensity of the laser beam (300 mW), in combination with rapid oscillations of the milling assembly and constant mixing of the reaction mixture, ensure negligible influence of laser radiation to reaction mixture. Spectral resolution is $4\,\mathrm{cm}^{-1}$, which gives distance between subsequent points in the resulting spectrum $\Delta\tilde{\nu} = 2\,\mathrm{cm}^{-1}$. For each spectrum, 20 scans of 1 s were averaged, which gave $\Delta t = 20\,\mathrm{s}$ time resolution.

Characterisation

IR spectra are acquired in argon-filled glove box, by Bruker Alpha spectrometer equipped with Platinum ATR accessory (single-reflection IIIa type diamond with 2×2 mm facet). The nominal resolution is $4\,\mathrm{cm}^{-1}$, and each spectrum was taken as an average of 10 co-added Fourier-transformed interferograms (scans).

Raman spectra of samples DLMAB and DSMAB were recorded using a Bruker Senterra Raman microscope. As a source, the instrument uses a 532 nm laser. Spectral resolution was set to $5\,\mathrm{cm}^{-1}$, while spatial resolution was $< 5\,\mu\mathrm{m}$.

X-ray powder diffractograms (XRD) of the samples in a $\phi = 1\,\mathrm{mm}$ capillary were recorded at 30 °C using a Bruker D8 Advance diffractometer with Cu anode. The 2Θ range was $10 - 90^\circ$ with a $\Delta(2\Theta) = 0.0221^\circ$ step and counting time per step was 492.02 ms. The simulated annealing was run until a plausible structure where Mg atoms were found coordinated by four N atoms and Li atoms coordinated by hydrogen atoms of the BH_3 moiety. The structure model was refined using the Rietveld method, together with unit cell parameters, coefficients of the shifted Chebyshev polynomial used to describe background, peak position, and shape parameters. All calculation were performed using the program Topas.[35]

Thermogravimetric and differential thermal analysis (TG/DTA) was performed simultaneously with a Mettler Toledo TA 4000 system. Measurements were done under N_2 flow at a rate of $50\,\mathrm{mL\,min}^{-1}$, in the $25 - 200\,^\circ\mathrm{C}$ range. Heating rate was $2\,^\circ\mathrm{C\,min}^{-1}$.

The differential scanning calorimetry (DSC) measurements was conducted by SETARAM DSC131 evo device. Measurements were done in temperature range from 30 to 200 °C, with heating rate of $2\,^\circ\mathrm{C\,min}^{-1}$, under constant N_2 flow. Enthalpies of solid-state phase changes are calculated from areas under Lorentzian functions fitted to individual thermal events of DSC profiles. From these areas, enthalpy change of the first and second dehydrogenation are obtained using the equation:

$$\Delta H = \frac{M S_{\mathrm{peak}}}{\beta} \tag{1}$$

where M is molar mass of initial compound in $\mathrm{g\,mol}^{-1}$, S_{peak} is area under DSC peak in $\mathrm{K\,W\,s}^{-1}$ and β is ramping rate in $\mathrm{K\,s}^{-1}$.

To analyze the composition of gaseous products (EGA) of thermal dehydrogenation of samples, a home-made setup for temperature programmed desorption (TPD) coupled with an Extorr 3000 quadrupole mass spectrometer (MS) was used. It uses up to 5 mg of powdered sample in quartz tube, placed inside an electrical furnace. Prior to measurement, the tube with sample was outgassed at room temperature and 10^{-7} torr. After that, the sample was linearly heated at $10\,^\circ\mathrm{C\,min}^{-1}$ from room temperature to 200 °C. The EGA signals, as partial pressures, at 8 different m/z ratios were followed and simultaneously recorded as a function of temperature. The observed m/z ratios were: 1 (H), 2 (H_2), 17 (NH_3 or OH), 18 (H_2O), 28 (B_2H_6), 43 (μ-$(NH_2)B_2H_5$), 58 (cyclo-$(NH_2BH_2)_2$), 81 (cyclo-$(NHBH)_3$).

3 Results and discussion

3.1 Preparation of $M_2Mg(AB)_4$

Mechanochemical preparation of $Na_2Mg(AB)_4$ (DSMAB) using planetary mill, directly from the corresponding stoichiometric mixture of NaH, MgH_2 and AB was previously reported.[17] Since we use a high-energy mill-shaker for ball milling reactions, we checked the applicability of this mill to repeat the reported reaction. Both IR spectra and XRD patterns (Fig. 1) confirm that this synthesis was successfully repeated. This allows the application of the same conditions to obtain the $Li_2Mg(AB)_4$ (DLMAB). The general chemical reaction of the preparation of $M_2Mg(AB)_4$ is:

$$2\,MH + MgH_2 + 4\,NH_3BH_3 \longrightarrow M_2Mg(NH_2BH_3)_4 + 4\,H_2 \tag{2}$$

where M = Li or Na. 30 min milling of the stoichiometric mixture of LiH, MgH_2 and AB resulted in a product. The similarity of IR and Raman spectra of obtained product with those for DSMAB (Fig. 1, Table 1) indicates the successfully prepared DLMAB.

3.2 Structure and composition

Although DSMAB and DLMAB have very similar IR and Raman spectra, their XRD patterns are very different. (Fig. 1). This indicates that crystallographically they are not isostructural, although M and Mg atoms are equally coordinated in both systems (Fig. 1).

The diffraction pattern of DLMAB was indexed using an orthorhombic unit cell which left several peaks unindexed. The quality of the Pawley fit however, suggested that these may be due to impurities. Parts of the pattern with major impurity peaks were at first excluded. The crystal structure of DLMAB was solved in direct space by simulated annealing taking the amidoborane moiety as a rigid body. The Li and Mg atoms were treated as independent atoms.

Rietveld fitting of the powder XRD for DLMAB (Fig. 2) shows that it crystallises in the orthorhombic *Pbcn* space group with one lithium atom, two AB moieties and $1/2$ of Mg atom comprising the asymmetric unit satisfying the overall charge neutrality. The Mg atom lies on the second order axis (Wyckoff position *c* in the *Pbcn* space group). In DLMAB, analogous to DSMAB,[17] magnesium is tetrahedrally coordinated by nitrogen atoms of the amido groups while lithium is coordinated by hydrogen atoms of the BH_3 moiety, in a distorted coordination environment (Fig. 3). Thus, coordination of metal atoms in DLMAB is analogous to that in DSMAB. However, packing is significantly different in these two systems.

This is further consolidated by Rietveld analysis (Fig. 2), which shows that diffractogram for both DLMAB and DSMAB are fully described by predominant $M_2Mg(AB)_4$ phase, with a contribution of long-chain $M(BH_3NH_2BH_2NH_2BH_3)$ (further in the text denoted as M(B3N2)) phase[36] and MgH_2[37] (Fig. 2). Attribution of diffraction patterns for both DLMAB and DSMAB to

these three-phase systems provided an excellent fit to the experimental data (Figs. 2 and S1-S3). The appearance of Na(B3N2) phase during mechanochemical synthesis has been already reported.[17] Even more interesting, $Na_2Mg(AB)_4$, as prepared in THF solution from NaH, $Mg(NH_2)_2$ and AB, also contains this phase.[13] Practically the equal intensity ratio of XRD peaks for sample prepared by ball milling with respect of that prepared in solution indicates that the equal mechanism takes place irrespectively of the preparation method.[13,17]

3.3 Mechanistic considerations

In order to reveal the reaction pathway through which amidoboranes are prepared by milling, as well as the emergence and development of observed M(B3N2) species, we used Raman spectroscopy to monitor ball milling reactions in-situ (Figs. S4 and S5, see ESI). Unfortunately, the intensity of the overall spectra is relatively low, allowing only $\nu(\mathrm{BH})$ region to be accurately analysed. First, a strong band due to PMMA reaction vessel in the $3200-2650\,\mathrm{cm}^{-1}$ range completely overlaps the $\nu(\mathrm{NH})$ region (see the ESI for illustrative example). On the other hand, the bands lying in the fingerprint region are of low intensity, disabling accurate intensity measurements. Thus, further considerations are based exclusively on measurements of the $\nu(\mathrm{BH})$ envelope by fitting it to appropriate Lorentzian profile functions.

The spectrum of $2\,\mathrm{NaH}+\mathrm{MgH_2}+4\,\mathrm{AB}$ reaction, as taken at $t=0\,\mathrm{min}$, differs from AB in a significant reduction of overall intensity, as well as appearance of a prominent feature at $2188\,\mathrm{cm}^{-1}$ and weak bands at 2103 and $2067\,\mathrm{cm}^{-1}$. This undoubtedly shows that a new phase is produced immediately when NaH come into touch with AB. The molar ratio of the reactants (NaH : AB = 1 : 2), comparison with available spectra, as well as the behaviour of the $2\,\mathrm{LiH}+\mathrm{MgH_2}+4\,\mathrm{AB}$ system, altogether indicates that an intermediate species of $\mathrm{NaNH_2BH_3\cdot NH_3BH_3}$ (Na(AB)·AB) composition is produced at this stage (Fig. 4). In these spectra, clear $2315\,\mathrm{cm}^{-1}$ band of Na(AB)·AB is represented as a shoulder, which is explainable by lower resolution of in-situ spectra, as well as the band broadening due to the dynamic conditions in which the spectra are acquired. At best of our knowledge, Na(AB)·AB is not reported since, but detailed description of this species is out of the scope of present paper.

The initial reaction of AB with LiH is significantly slower with respect to NaH. Spectrum, as taken at $t=0\,\mathrm{min}$, shows that the reaction mixture consists of intact reagents AB, LiH and $\mathrm{MgH_2}$ (Fig. 5). In the first 10 min of milling an intermediate phase is produced (Figs. 5 and 6(b)). This phase is represented in Raman spectra with 2368 and $2325\,\mathrm{cm}^{-1}$ bands, as well as a broad shoulder at $2195\,\mathrm{cm}^{-1}$, with preservation of strong $2281\,\mathrm{cm}^{-1}$ band. Fig. S6 (see ESI), shows evolution of position of the $\nu_{as}(\mathrm{BH})$ band. It clearly shows that, although the development of new bands is evident (Fig. 5), this particular vibration is not significantly affected by initial reaction. The molar ratio of LiH and AB, as well as low reactivity of $\mathrm{MgH_2}$ with AB, indicates the formation of $\mathrm{LiNH_2BH_3\cdot NH_3BH_3}$ intermediate phase (further in the text Li(AB)·AB) at this stage. In order to check this hypothesis, we reproduced the previously reported synthesis of Li(AB)·AB adduct.[38] Comparison of XRD patterns (ESI) proves

this route. Thus, the following reaction represents the first step in the production of intermediate $M_2Mg(AB)_4$ (M = Li or Na):

$$MH + 2\,AB \xrightarrow{B.M.} M(AB)\cdot AB_{(s)} + H_{2(g)} \tag{3}$$

The intensities of the spectral features attributed to $M(AB)\cdot AB$ phases suffer a steep decrease, simultaneously with increase of new features (Figs. 4 and 5). The most characteristic band for both species appears at $2230\,cm^{-1}$ and this is used to follow the evolution of the product (black dots in Fig. 6). However, at this stage the $\nu_{as}(BH)$ band (Fig. S6, see ESI) shifts toward the lower wavenumbers, reflecting a significant weakening of the B−H bond due to the reaction of $M(AB)\cdot AB$ with MgH_2. Indeed, structural parameters (Table S1, see ESI) show significantly longer B−H band in $M_2Mg(AB)_4$ systems with respect of AB. Thus, the intermediate species, produced by eq. (3), are prerequisite for further reaction with MgH_2, giving the final product $M_2Mg(AB)_4$:

$$2M(AB)\cdot AB + MgH_2 \xrightarrow{B.M.} M_2Mg(AB)_{4(s)} + 2H_{2(g)} \tag{4}$$

This reaction takes place simultaneously with formation of $M(AB)\cdot AB$ intermediate phase, and it includes substitution of M^+ with Mg^{2+}, forming Mg−N bonds with coordination of Li^+ or Na^+ with BH groups through hydride hydrogens.

Interesting, in both cases, a significant drop of intensities of all the spectral features is observed, which reflects glueing of the reaction mixture (green lines in Fig. 6). After some time, the spectra reappear. This behaviour indicates formation of a Mg-containing intermediate phases. On the basis of available experimental data we can not deduce the composition of this intermediate phase. At this stage we can only speculate about complexation of Mg^{2+} (or MgH_2) with $M(AB)\cdot AB$. These instable species readily rearranges into final $M_2Mg(AB)_4$. This hypothesis seems reasonable, since, according to molecular structure of DSMAB [17] and DLMAB (Fig. 3) with respect of Li(AB) and Na(AB),[10] Mg^{2+} substitute M^+ covalently bonded with N of AB and extrude it to coordinate with BH moiety. However, the confirmation of this hypothesis, as well as elucidation of the structure of this intermediate is out of scope of the present study.

In both cases, after the reappearence of the spectra, intensity of the $2230\,cm^{-1}$ reaches the plateau (Fig. 6). After this step, no further spectral changes are observed, indicating formation of the final products and consequent termination of the reactions. In order to check this, IR spectrum and XRD of the sample DSMAB after 90 min of milling, are compared with those previously published,[17] which confirms formation of $Na_2Mg(AB)_4$, as well as $Li_2Mg(AB)_4$. Fig. 6 also shows that the reaction of MgH_2 with $Li(AB)\cdot AB$ is $\sim 1.5\times$ faster than with $Na(AB)\cdot AB$, as determined by fitting of the linear part of the $I(2230\,cm^{-1}) = f(t)$ and duration of the 'sticky' intermediate phase, in accordance with the evidence of generally higher reactivity of Li-containing compounds.[39]

The presence of M(B3N2) is confirmed by analysis of powder XRD (see Fig. 2 for DLMAB).[36,40] Also, Raman spectra show that the features attributable to M(B3N2) species arise soon after the start mechanochemical synthesis, following the production

of M(AB)·AB, and these features persist over the rest of the reaction. This shows that the reaction of M(AB)·AB with MgH_2 (4) is in competition with:

$$M(AB)\cdot AB + AB \xrightarrow{\Delta} M(B3N2)_{(s)} + NH_{3(g)} + H_{2(g)} \quad (5)$$

the presence of NH_3 in reaction vessels at the end of reaction further supports this interpretation. Eventual excess AB is completely consumed by reaction (5), which proceeds in the first phase of the synthesis, and this process is in competition with reaction that include MgH_2, giving rise to DLMAB.

Let us consider the observation that the Na(B3N2) phase is produced regardless of the reaction conditions, i.e. it is observed in the same amount from XRD of DSMAB prepared from THF solution of NaH, MgH_2 and AB [13] and by ball milling, [17] as repeated here. This strongly indicates the same mechanistic pathway, which is independent of reaction medium. In this reaction, THF acts exclusively as a solvent which does not affect the reaction by itself. In the other words, it only enables molecular mobility, which is driving force of the reaction in the same way as transfer of energy by balls in mechanochemical approach. In both cases, Na(AB)·AB is produced by reaction (3) in the first step, and the formed intermediate phase further reacts through (4) giving the $Na_2Mg(AB)_4$ as a dominant product. However, the side reaction (5) is also evident in both cases, resulting in Na(B3N2). Although the absolute rate of first and second step of this reaction can vary with respect of reaction conditions, ratio of rates of reactions involved in the second step is insensitive to applied conditions.

3.4 Thermal dehydrogenation

TG reveals a two-step H_2 release from DSMAB [17] at 137 and 171 °C and in a minor extent at 85 °C at 2 °C min^{-1} heating rate. In the case of DLMAB, a small loss of the mass around 85 °C is observed. As seen from comparison of TPD with derivative of TG for DLMAB (Fig. 7), TG is well correlated with emission of H_2, confirming that its thermal decomposition is accompanied by release of hydrogen as a predominant gaseous product.

Phase transformations of $M_2Mg(AB)_4$ from room temperature to 200 °C were followed by DSC (Figure 7). DSMAB shows several distinct features: endothermic process in the temperature range $40-70$ °C with a maximum at 60 °C, followed by three exothermic processes as listed in Table 2 and shown in Figs. S7 and S8 (see ESI). The endothermic reaction preceding thermal decomposition is characteristic for Na and Li amidoboranes. [41] Weak endothermic DSC peak can be attributed to melting or amorphization of the mixture. [42], eventually yielding species containing $M(NH_3)^+$ cations. [41] Here suggested synthetic route lead to formation of Li-containing system with DSC profile given in Fig. 7. Observed exothermic processes occur at lower temperatures than those for pure AB [11] and AB/MgH_2 mixture. [43] In contrast to results of Nakagawa et al. [42], who have observed three exothermic peaks at 53, 117 and 131 °C in $AB/LiAlH_4$ system, DSC analysis of DLMAB sample reveals two additional processes at 80 and 151 °C.

The obvious difference in TPD-MS and DSC curves is due to the difference in thermodynamic driving force, [44,45] i.e. exper-

imental conditions. DSMAB (Fig. 7 and Table 2) shows three desorption maxima. TPD-MS analysis shows that hydrogen is generated as a consequence of both high-temperature chemical conversions. The process taking place at 93 °C is accompanied by NH_3 emission. In both DLMAB and DSMAB case, NH_3 is released in amount of < 1 % in total gas, which is consistent with calculated very high deammoniation energies with respect to those for dehydrogenation.[19] However, DLMAB releases somewhat more NH_3 with respect to DSMAB, which is also consistent with the observed trends. In the $130-180$ °C region, three maxima (Table 2, Figs. S9 and S10, see ESI) are observed, in accordance with previously published results.[46] At this stage, we can assume that this is caused by formation of M(B3N2) phase. Although this species is undoubtedly observed in our material, further studies are required to confirm this hypothesis.

At the current stage, our observations and measured dehydrogenation energies (Table 2) are consistent with dehydrogenation mechanism for bimetallic Mg-containing amidoboranes as proposed and computationally analysed.[15,19,47] In the other words, the decomposition mechanism involves intermolecular production of H_2 through alkaline hydride-mediated oligomerisation of the neighbouring $[NH_2BH_3]^-$ groups by $BH^{\delta-}\cdots{}^{+\delta}HN$ dihydrogen bonding interaction. The hydride H^- from BH_3 groups of $[NH_2BH_3]^-$ moiety is transfered to Na^+ or Li^+ forming alkaline hydride MH, which subsequently interacts with protic H^+ of the $Mg(NH_2BH_3)_4{}^{2-}$ group. H_2 is released as a consequence of this reaction. Since the formation of new B−N bond is exothermic process, while bond breaking is endothermic process, it results in relatively small total value of dehydrogenation ΔH.

4 Conclusions

The present results provide a new entry for a systematic understanding and rational control of mechanochemical preparation of systems for solid-state hydrogen storage. The novel mixed-metal amidoborane $Li_2Mg(AB)_4$ (DLMAB) has been prepared by direct ball milling of the reaction mixture $(2\,LiH + MgH_2 + 4\,AB)$, in a way similar to its Na-containing analogue (DSMAB). The crystal structure of DLMAB was determined from powder XRD and refined using the Rietveld method. Coordination of metal atoms is equal to that for DSMAB, i.e. each Mg^{2+} is tetrahedrally coordinated with N atoms of NH_2BH_3 moieties, while Li^+ forms distorted octahedra through 6 Li−H−B coordination bonds. Although bonding and coordination are similar for the two systems, crystal packing of DLMAB significantly differs from DSMAB.

To the best of our knowledge, here is for the first time employed in-situ Raman spectroscopy for uninterrupted, real-time monitoring of mechanochemical preparation of hydrogen storage materials. For both DLMAB and DSMAB, a two-step reaction pathway is revealed, where LiH or NaH first react with AB, giving intermediate $M(AB)\cdot AB$ species. In the second step, it reacts with MgH_2, giving $M_2Mg(AB)_4$. However, this second step is in competition with a side-reaction leading to $M(BH_3NH_2BH_2NH_2BH_3)$, resulting in a moderate contamination of the final products. This byproduct phase is produced irrespectively of reaction conditions. It is demonstrated that DLMAB releases pure H_2 in the 7 wt% amount, with trace amounts of NH_3 and B_2H_6 contamination, and no detectable borazine. Although the detailed desorption mechanism of both phases is still

unknown and needs to be further investigated in detail, the results are highly consistent with previously proposed mechanism that involves intermolecular oligomerisation through the interaction of neighbouring $NH_2BH_3^-$ groups. At this stage we can conclude that DLMAB would be a potential candidate for PEM fuel cell vehicle applications.

Acknowledgements

This work was supported by the Ministry of Environment and Energy, the Ministry of Science and Education, the Environmental Protection and Energy Efficiency Fund and the Croatian Science Foundation under the project "New Materials for Energy Storage", in the total amount of 1 962 100.00 HRK, and by MEST of Serbia under grant III45012. It arose in the framework of the Serbian-Croatian bilateral project "Ammonia Borane and Its Derivatives for Solid-State Hydrogen Storage", and a part of this work was realised in the framework of the COST Action MP1103 "Nanostructured materials for solid-state hydrogen storage". We are indebted to Mr. Vitomir Stanišić and his team from the workshop of the Ruđer Bošković Institute for their continuous support. NB wishes to thank Foundation "Knowledge in Action", which enabled workshop for high school students of several high schools from Zagreb in his Laboratory (list of schools and students is given in ESI). We are grateful to Zoran Jovanović for TPD measurements.

Associated content

Crystal structure of DLMAB (CCDC 432929); Rietveld fit of the XRD pattern of DSMAB and DLMAB; structure parameters; 2D representations of in-situ Raman spectra of ball milling preparations of DSMABand DLMAB; DSC and TPD-MS profiles; List of schools and high school students who contributed in mechanochemical preparations of the samples.

References

[1] Luo, J.-H., Kang, X.-D., and Wang, P. (2010) Mechanically Milling with Off-the-Shelf Magnesium Powder to Promote Hydrogen Release from Ammonia Borane. *The Journal of Physical Chemistry C 114*, 10606–10611.

[2] Yuan, P. F., Wang, F., Sun, Q., Jia, Y., and Guo, Z. X. (2013) Dehydrogenation mechanisms of $Ca(NH_2BH_3)_2$: The less the charge transfer, the lower the barrier. *Int. J. Hydrogen En. 38*, 11313 – 11320.

[3] Gutowska, A., Li, L., Shin, Y., Wang, C. M., Li, X. S., Linehan, J. C., Smith, R. S., Kay, B. D., Schmid, B., Shaw, W., Gutowski, M., and Autrey, T. (2005) Nanoscaffold Mediates Hydrogen Release and the Reactivity of Ammonia Borane. *Angew. Chem. Int. Ed. Engl. 44*, 3578–3582.

[4] Bluhm, M. E., Bradley, M. G., Butterick III, R., Kusari, U., and Sneddon, L. G. (2006) Amineborane-Based Chemical Hydrogen Storage: Enhanced Ammonia Borane Dehydrogenation in Ionic Liquids. *J. Am. Chem. Soc. 128*, 7748–7749.

[5] Feaver, A., Sepehri, S., Shamberger, P., Stowe, A., Autrey, T., and Cao, G. (2007) Coherent Carbon CryogelAmmonia Borane Nanocomposites for H2 Storage. *J. Phys. Chem. B 111*, 7469–7472.

[6] Neiner, D., Luedtke, A., Karkamkar, A., Shaw, W., Wang, J., Browning, N. D., Autrey, T., and Kauzlarich, S. M. (2010) Decomposition Pathway of Ammonia Borane on the Surface of Nano-BN. *J. Phys. Chem. C 114*, 13935–13941.

[7] Stephens, F. H., Pons, V., and Baker, R. T. (2007) Ammoniaborane: the hydrogen source par excellence? *Dalton Trans.* 2613–2626.

[8] Denney, M. C., Pons, V., Hebden, T. J., Heinekey, D. M., and Goldberg, K. I. (2006) Efficient Catalysis of Ammonia Borane Dehydrogenation. *J. Am. Chem. Soc. 128*, 12048–12049.

[9] Keaton, R. J., Blacquiere, J. M., and Baker, R. T. (2007) Base Metal Catalyzed Dehydrogenation of AmmoniaBorane for Chemical Hydrogen Storage. *J. Am. Chem. Soc. 129*, 1844–1845.

[10] Xiong, Z., Yong, C. K., Wu, G., Chen, P., Shaw, W., Karkamkar, A., Autrey, T., Jones, M. O., Johnson, S. R., Edwards, P. P., and David, W. I. F. (2008) High-Capacity Hydrogen Storage in Lithium and Sodium Amidoboranes. *Nature Mater. 7*, 138–141.

[11] Biliškov, N., Vojta, D., Kótai, L., Szilágyi, I. M., Hunyadi, D., Pasinszki, T., Flinčec Grgac, S., Borgschulte, A., and Züttel, A. (2016) High Influence of Potassium Bromide on Thermal Decomposition of Ammonia Borane. *J. Phys. Chem. C 120*, 25276–25288.

[12] Chua, Y. S., Chen, P., Wu, G., and Xiong, Z. (2011) Development of Amidoboranes for Hydrogen Storage. *Chem. Commun. 47*, 5116–5129.

[13] Chua, Y. S., Li, W., Wu, G., Xiong, Z., and Chen, P. (2012) From Exothermic to Endothermic Dehydrogenation Interaction of Monoammoniate of Magnesium Amidoborane and Metal Hydrides. *Chem. Mater. 24*, 3574–3581.

[14] Staubitz, A., Robertson, A. P. M., and Manners, I. (2010) Ammonia-Borane and Related Compounds as Dihydrogen Sources. *Chem. Rev. 110*, 4079–4124.

[15] Kim, D. Y., Lee, H. M., Seo, J., Shin, S. K., and Kim, K. S. (2010) Rules and trends of metal cation driven hydride-transfer mechanisms in metal amidoboranes. *Phys. Chem. Chem. Phys. 12*, 5446–5453.

[16] Luedtke, A. T., and Autrey, T. (2010) Hydrogen Release Studies of Alkali Metal Amidoboranes. *Inorg. Chem. 49*, 3905–3910.

[17] Wu, H., Zhou, W., Pinkerton, F. E., Meyer, M. S., Yao, Q., Gadipelli, S., Udovic, T. J., Yildirim, T., and Rush, J. J. (2011) Sodium magnesium amidoborane: the first mixed-metal amidoborane. *Chem. Commun. 47*, 4102–4104.

[18] Owarzany, R., Leszczyński, P. J., Fijalkowski, K. J., and Grochala, W. (2016) Mono- and Bimetalic Amidoboranes. *Crystals* 88.

[19] Wang, K., Zhang, J. G., Li, T., Liu, Y., Zhang, T., and Zhou, Z. N. (2015) Electronic structures and dehydrogenation properties of bimetallic amidoboranes. *Int. J. Hydrogen En. 40*, 2500 – 2508.

[20] Kang, X., Luo, J., Zhang, Q., and Wang, P. (2011) Combined formation and decomposition of dual-metal amidoborane $NaMg(NH_2BH_3)_3$ for high-performance hydrogen storage. *Dalton Trans. 40*, 3799–3801.

[21] Kang, X., Wu, H., Luo, J., Zhou, W., and Wang, P. (2012) A simple and efficient approach to synthesize amidoborane ammoniates: case study for $Mg(NH_2BH_3)_2(NH_3)_3$ with unusual coordination structure. *J. Mater. Chem. 22*, 13174–13179.

[22] Chua, Y. S., Wu, H., Zhou, W., Udovic, T. J., Wu, G., Xiong, Z., Wong, M. W., and Chen, P. (2012) Monoammoniate of Calcium Amidoborane: Synthesis, Structure, and Hydrogen-Storage Properties. *Inorg. Chem. 51*, 1599–1603.

[23] James, S. L. et al. (2012) Mechanochemistry: opportunities for new and cleaner synthesis. *Chem. Soc. Rev. 41*, 413–447.

[24] Tumanov, I. A., Achkasov, A. F., Boldyreva, E. V., and Boldyrev, V. V. (2011) Following the products of mechanochemical synthesis step by step. *Cryst. Eng. Commun. 13*, 2213–2216.

[25] Friščić, T., Halasz, I., Beldon, P. A., Belenguer, A. M., Adams, F., Kimber, S. A. J., Honkimäki, V., and Dinnebier, R. E. (2013) Real-time and in situ monitoring of mechanochemical milling reactions. *Nature Chem. 5*, 66–73.

[26] Halasz, I., Puškarić, A., Kimber, S. A. J., Beldon, P. J., Belenguer, A. M., Adams, F., Honkimäki, V., Dinnebier, R. E., Patel, B., Jones, W., Štrukil, V., and Friščić, T. (2013) Real-time in situ powder X-ray diffraction monitoring of mechanochemical synthesis of pharmaceutical cocrystals. *Angew. Chem. Int. Ed. 52*, 11538–11541.

[27] Halasz, I., Kimber, S. A. J., Beldon, P. J., Belenguer, A. M., Adams, F., Honkimäki, V., Nightingale, R. C., Dinnebier, R. E., and Friščić, T. (2013) In situ and real-time monitoring of mechanochemical milling reactions using synchrotron X-ray diffraction. *Nature Prot. 8*, 1718–1729.

[28] Gracin, D., Štrukil, V., Friščić, T., Halasz, I., and Užarević, K. (2014) Laboratory Real-Time and In Situ Monitoring of Mechanochemical Milling Reactions by Raman Spectroscopy. *Angew. Chem. Int. Ed. 53*, 6193–6197.

[29] Juribašić, M., Užarević, K., Gracin, D., and Ćurić, M. (2014) Mechanochemical CH bond activation: rapid and regioselective double cyclopalladation monitored by in situ Raman spectroscopy. *Chem. Commun. 50*, 10287–10290.

[30] Tireli, M., Juribašić Kulcsar, M., Cindro, N., Gracin, D., Biliškov, N., Borovina, M., Ćurić, M., Halasz, I., and Užarević, K. (2015) Mechanochemical Reactions Studied by In Situ Raman Spectroscopy: Base Catalysis in Liquid-Assisted Grinding. *Chem. Commun. 51*, 8058–8061.

[31] Katsenis, A. D., Puškarić, A., Štrukil, V., Mottillo, C., Julien, P. A., Užarević, M. H., K. Pham, Do, T. O., Kimber, S. A. J., Lazić, P., Magdysyuk, O., Dinnebier, R. E., Halasz, I., and Friščić, T. (2015) In situ X-ray diffraction monitoring of a mechanochemical reaction reveals a unique topology metal-organic framework. *Nature Commun. 6*, 6662.

[32] Batzdorf, L., Fischer, F., Wilke, M., Wenzel, K. J., and Emmerling, F. (2015) Direct InSitu Investigation of Milling Reactions Using Combined X-ray Diffraction and Raman Spectroscopy. *Angew. Chem. Int. Ed. 54*, 1799–1802.

[33] Kurko, S., Matović, L., Novaković, N., Matović, B., Jovanović, Z., Paskaš Mamula, B., and Grbović Novaković, J. (2011) Changes of hydrogen storage properties of MgH_2 induced by boron ion irradiation. *Int. J. Hydrogen En. 36*, 1184 – 1189.

[34] Autrey, T., Gutowska, A., Li, L., Linehan, J., and Gutowski, M. (2004) Chemical hydrogen storage in nano-structured materials. Control of hydrogen release and reactivity from ammonia borane complexes. *ACS Div. Fuel Chem., Prepr. 49*, 150–151.

[35] Bruker-AXS, (2009) Topas version 4.2.

[36] Fijalkowski, K. J., Jaron, T., Leszczynski, P. J., Magos-Palasyuk, E., Palasyuk, T., Cyranski, M. K., and Grochala, W. (2014) $M(BH_3NH_2BH_2NH_2BH_3)$ - the Missing Link in the Mechanism of the Thermal Decomposition of Light Alkali Metal Amidoboranes. *Phys. Chem. Chem. Phys. 16*, 23340–23346.

[37] Moriwaki, T., Akahama, Y., Kawamura, H., Nakano, S., and Takemura, K. (2006) Structural Phase Transition of Rutile-Type MgH_2 at High Pressures. *J. Phys. Soc. Japan 75*, 074603.

[38] Wu, C., Wu, G., Xiong, Z., David, W. I. F., Ryan, K. R., Jones, M. O., Edwards, P. P., Chu, H., and Chen, P. (2010) Stepwise Phase Transition in the Formation of Lithium Amidoborane. *Inorg. Chem. 49*, 4319–4323.

[39] Dovgaliuk, I., Jepsen, L. H., Safin, D. A., Łodziana, Z., Dyadkin, V., Jensen, T. R., Devillers, M., and Filinchuk, Y. (2015) A Composite of Complex and Chemical Hydrides Yields the First Al-Based Amidoborane with Improved Hydrogen Storage Properties. *Chem. Eur. J. 21*, 14562–14570.

[40] Owarzany, R., Fijalkowski, K. J., Jaroń, T., Leszczyński, P. J., Dobrzycki, L., Cyrański, M. K., and Grochala, W. (2016) Complete Series of Alkali-Metal M($BH_3NH_2BH_2NH_2BH_3$) Hydrogen-Storage Salts Accessed via Metathesis in Organic Solvents. *Inorg. Chem. 55*, 37–45.

[41] Fijalkowski, K. J., Genova, R. V., Filinchuk, Y., Budzianowski, A., Derzsi, M., Jaron, T., Leszczynski, P. J., and Grochala, W. (2011) Na[Li(NH_2BH_3)$_2$] the first mixed-cation amidoborane with unusual crystal structure. *Dalton Trans. 40*, 4407–4413.

[42] Nakagawa, Y., Shinzato, K., Nakagawa, T., Nakajima, K., Isobe, S., Goshome, K., Miyaoka, H., and Ichikawa, T. (2016) Synthesis, structural characterization, and hydrogen desorption properties of Na[Al(NH_2BH_3)$_4$]. *Int. J. Hydrogen En.*

[43] Kang, X., Ma, L., Fang, Z., Gao, L., Luo, J., Wang, S., and Wang, P. (2009) Promoted hydrogen release from ammonia borane by mechanically milling with magnesium hydride: A new destabilizing approach. *Phys. Chem. Chem. Phys. 11*, 2507–2513.

[44] Durojaiye, T., and Goudy, A. (2012) Desorption kinetics of lithium amide/magnesium hydride systems at constant pressure thermodynamic driving forces. *Int. J. Hydrogen En. 37*, 3298–3304.

[45] Pokol, G. (2000) The Thermodynamic Driving Force in the Kinetic Evaluation of Thermoanalytical Curves. *J. Therm. Anal. Calorim. 60*, 879–886.

[46] Nakagawa, Y., Isobe, S., Ikarashi, Y., and Ohnuki, S. (2014) AB-MH (Ammonia Borane-Metal Hydride) composites: Systematic understanding of dehydrogenation properties. *J. Mater. Chem. A 2*, 3926–3931.

[47] Wang, K., and Zhang, J.-G. (2013) Structural study and dehydrogenation mechanisms of a novel mixed metal amidoborane: Sodium magnesium amidoborane. *Chem. Phys. Lett. 590*, 27–34.

Tables and Figures

Table 1 IR and Raman spectra of DLMAB and DSMAB.

DLMAB		DSMAB		
IR	**Raman**	**IR**	**Raman**	**Assignation**[a]
3346 s	3347 s	3335 s	3336 s	$\nu_{as}(\mathrm{NH})$
3337 w	3338 m			
3321 w	3314 m			
3309 w		3301 m		$\nu_{as}(\mathrm{NH})^{b}$
3288 s	3290 vs	3284 m	3285 vs	$\nu_{s}(\mathrm{NH})$
3273 w	3272 m	3256 w	3256 m	$\nu_{s}(\mathrm{NH})^{b}$
2346 w	2358 w	2359 w	2358 w	$\nu_{as}(\mathrm{BH})^{b}$
2322 w	2322 m	2313 w	2322 w	$\nu_{as}(\mathrm{BH})$
2244 m	2249 m	2267 w		
2186 s	2222 vs	2205 vs	2230 vs	$\nu_{s}(\mathrm{BH})$
1570 w	1568 m	1556 w	1566 m	$\delta_{as}(\mathrm{NH_2})$
1544 s	1544 m	1541 m		
1375 w	1370 w	1415 w	1370 w	
1275 w	1275 m			
1232 m	1235 w	1241 m	1235 m	$\delta_{s}(\mathrm{NH_2})$
	1168 m	1164 m	1188 w	$\delta_{as}(\mathrm{BH_3})$
1152 m	1146 w	1153 w	1126 w	$\delta_{s}(\mathrm{BH_3})$
1044 m	1048 w	1049 m	1047 w	$\rho(\mathrm{NH_3})$
899 m	891 w			
880 m	872 m	880 m	849 m	$\nu(\mathrm{BN})$
825 w		826 w		
574 w		562 w		
545 w				
512 w		509 w		
438 w		449 w		

[a] According to Ref. [11]
[b] Degradation products, Ref. [36]

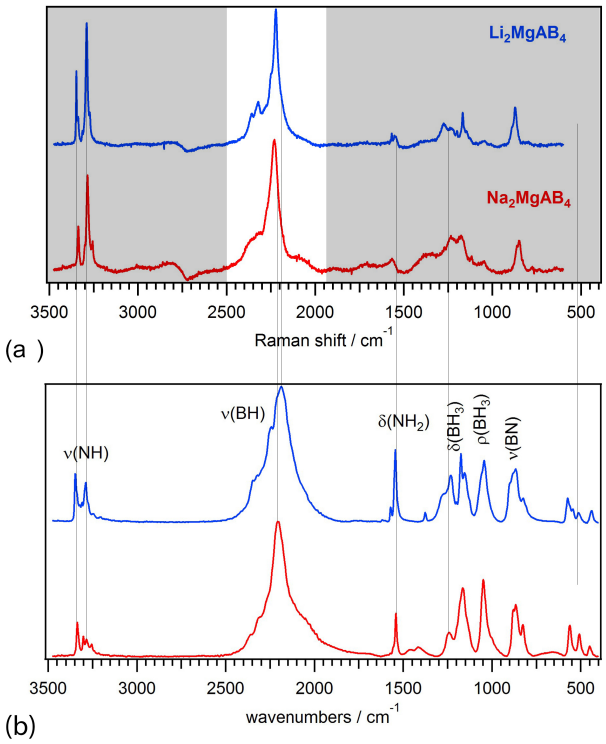

Figure 1 Comparison of DLMAB and DSMAB: (a) Raman spectra (white field denotes the observed spectral window around ν(BH) envelope); (b) IR spectra with approximate assignation.

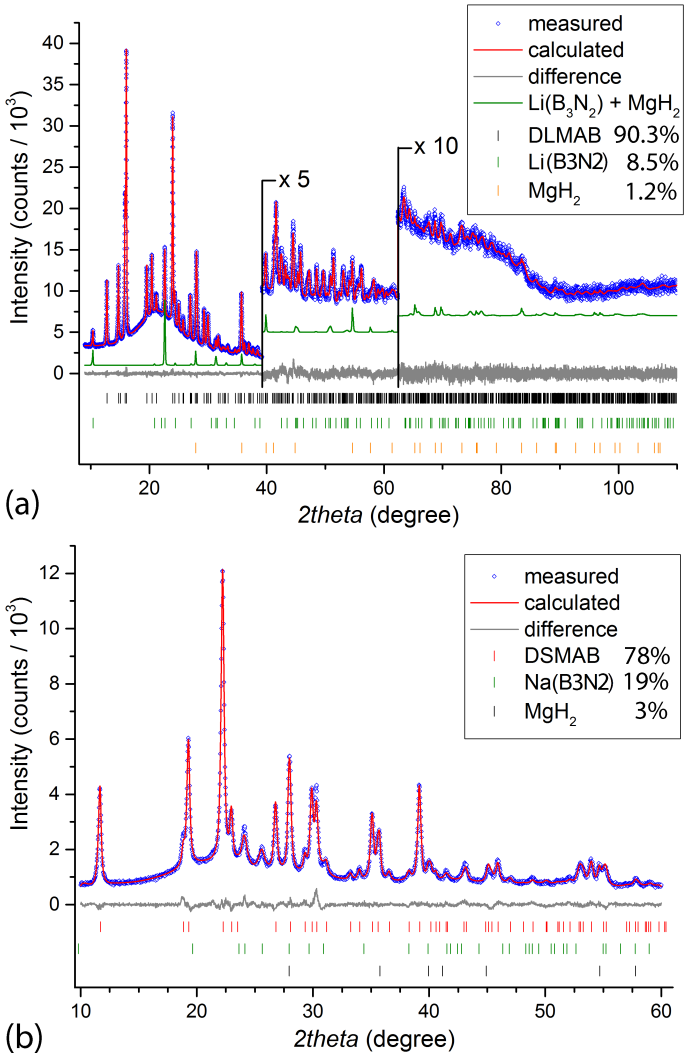

Figure 2 Quantitative composition of DLMAB and DSMAB samples, as determined from powder XRD patterns by fitting the patterns for (a) DLMAB and (b) DSMAB to MgH_2 [37] and M(B3N2) [36]. For analysis of DSMAB, $Na_2Mg(AB)_4$ was taken from ref. [17], while structure of $Li_2Mg(AB)_4$ was solved by Rietveld refinement.

Table 2 Temperatures of DSC and TPD-MS peaks, enthalpies of chemical transformations thet result in release of H_2 (calculated from areas below Gaussian profiles fitted to DSC curve) and quantity of released hydrogen as calculated from area under H_2 temperature desorption maxima, fitted to Lorentzian profiles.

DSMAB				**DLMAB**			
DSC		TPD		DSC		TPD	
t/°C	ΔH/kJ mol^{-1}	t/°C	%H_2	t/°C	ΔH/kJ mol^{-1}	t/°C	%H_2
thermal event not observed				56		60	0[a]
91	39.4 ± 0.5[b]	93	3	78		80	0[a]
146		135	27	116	30.1 ± 0.1[c]	103	29
162	48.4 ± 0.7[d]	—	—	126		—	—
170		166	22	150	29.9 ± 0.7[e]	160[f]	39

[a] Exclusively NH_3 detected by TPD-MS (Fig. 7).
[b] 1st dehydrogenation step for DSMAB (TPD event at 93 °C).
[c] 1st dehydrogenation step for DLMAB (TPD event at 103 °C).
[d] 2nd dehydrogenation step for DSMAB (TPD events in the 135 – 166 °C range).
[e] 2nd dehydrogenation step for DLMAB (TPD events in the 140 – 160 °C range).
[f] Sum of 156 and 162 °C feature (Fig. 7).

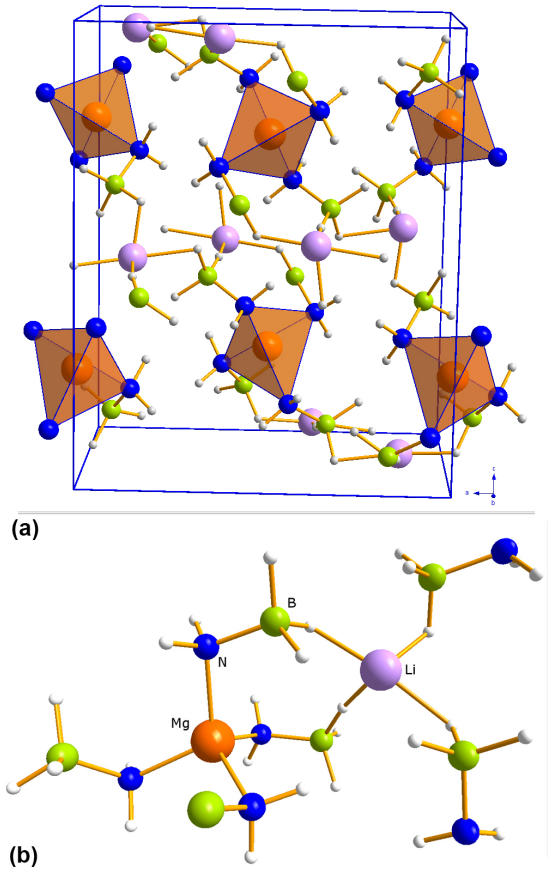

Figure 3 (a) Crystal packing and (b) bonding environment of DLMAB. Each Mg^{2+} is bind to four N^- forming a tetrahedron with $NH_2BH_3^-$ groups, and each Li^+ is octahedrally coordinated through six hydride H atoms of $NH_2BH_3^-$ moieties.

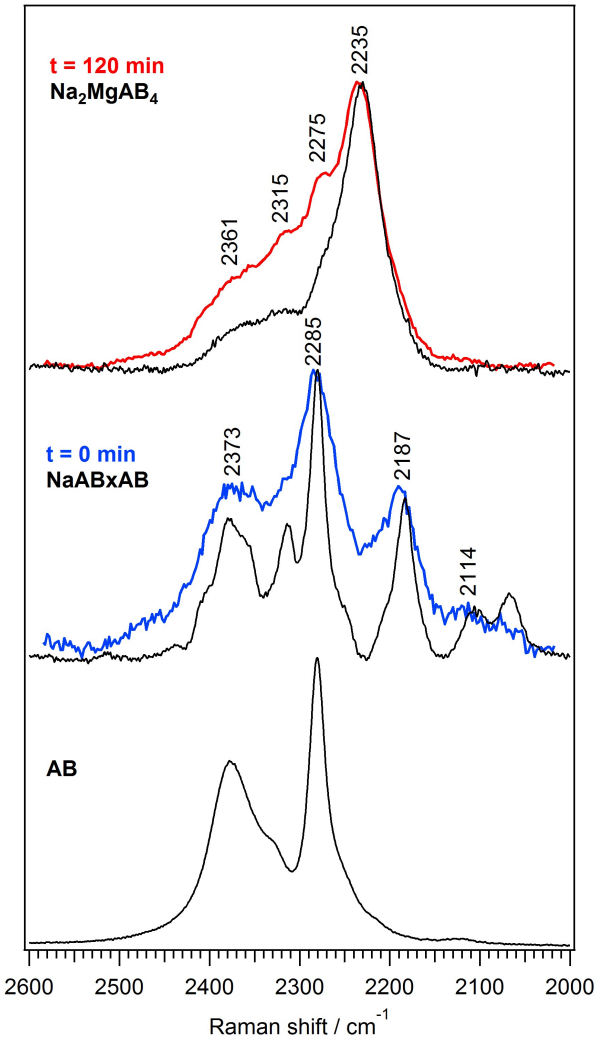

Figure 4 Representative Raman spectrum of the initial stage of reaction $2\,NaH + MgH_2 + 4\,AB$ and its comparison with AB and Na(AB)$\cdot$AB spectra.

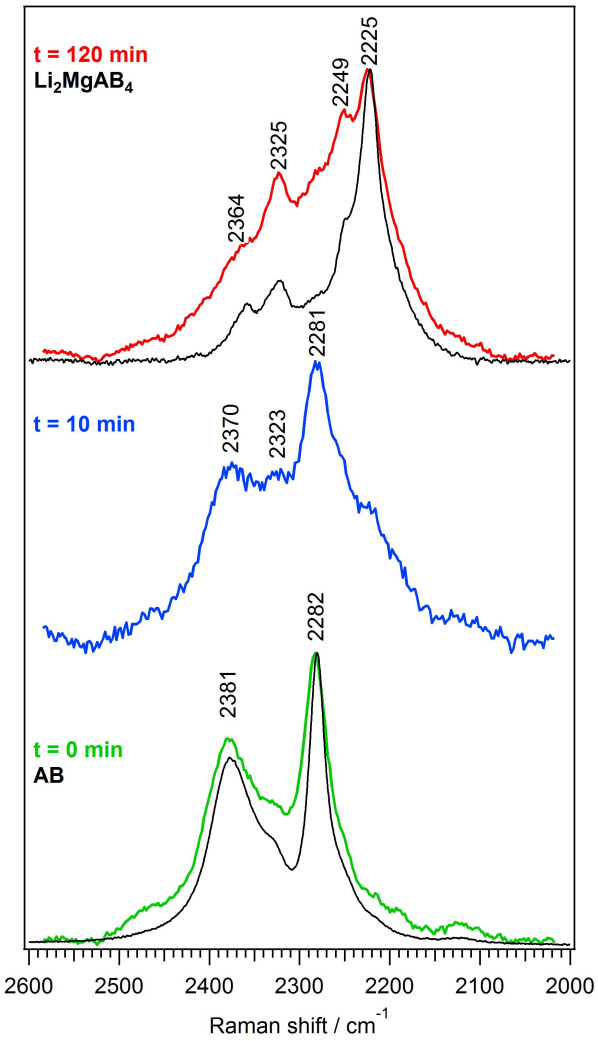

Figure 5 Representative Raman spectra as taken during the milling of $2\,\mathrm{LiH} + \mathrm{MgH_2} + 4\,\mathrm{AB}$ mixture and their comparison with AB and DLMAB.

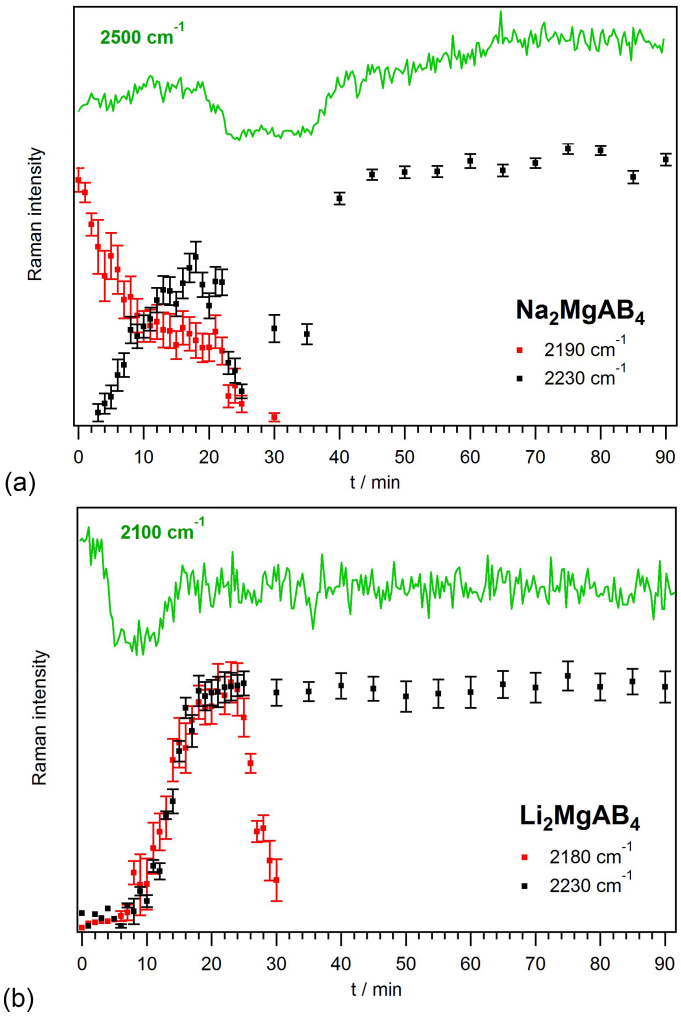

Figure 6 Temporal evolution of the M(AB)$\cdot$AB and $M_2Mg(AB)_4$ species ($2230\,cm^{-1}$) species as measured during the preparation of (a) DSMAB and (b) DLMAB by fitting the Raman band at ($2190\,cm^{-1}$) and ($2230\,cm^{-1}$), respectively, to Lorentzian profile function. Intensities, as shown here, are not in range. Green curves represents the behaviour of the low-intensity feature at $2500\,cm^{-1}$ for DSMAB and at $2100\,cm^{-1}$ for DLMAB, indicating the glueing of the reaction mixture to vessel during the milling.

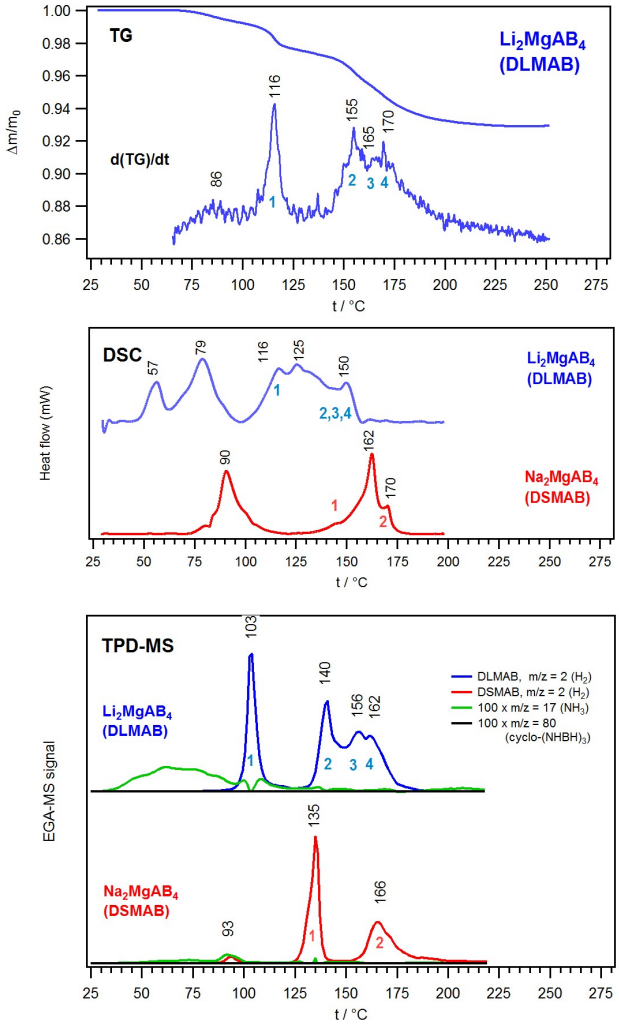

Figure 7 The TG, DSC and TPD-MS ($m/z = 2$ (H_2), 17 (NH_3, intensity multiplied by 100) and 81 ($(NHBH)_3$, intensity multiplied by 100) profiles for thermal decomposition of DLMAB and DSMAB. The individual H_2 desorption events are numbered.